Chemical Geology 644 (2024) 121869

Contents lists available at ScienceDirect

Chemical Geology

journal homepage: www.elsevier.com/locate/chemgeo

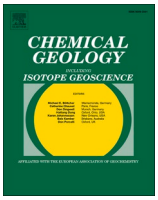

An in-situ experimental HP/HT study on bromine release from a natural basalt

Tobias Grützner [a,b,c,*], Hélène Bureau [a], Eglantine Boulard [a], Pascal Munsch [d], Nicolas Guignot [e], Julien Siebert [f], Yoann Guarnelli [a]

[a] Institut de Minéralogie, de Physique des Matériaux et de Cosmochimie (IMPMC), Sorbonne Université, Paris, France
[b] Research School of Earth Sciences, Australian National University, Canberra, Australia
[c] Institut für Geowissenschaften, Goethe-Universität Frankfurt, Germany
[d] Institut de Recherche en Astrophysique et Planétologie (IRAP), Toulouse, France
[e] Synchrotron SOLEIL, Saint-Aubin, France
[f] Institut de Physique du Globe de Paris, France

ARTICLE INFO

Editor: Claudia Romano

Keywords:
Bromine
Fluid/melt partitioning
Volcanic degassing
SXRF
Hydrothermal diamond anvil cell

ABSTRACT

We present the first in-situ partitioning data for bromine between a natural basaltic melt and a coexisting fluid. For this study hydrothermal diamond anvil cell experiments at pressures up to 1.7 GPa were conducted. We combined laser heating to melt the basalt glass with external heating to lower the temperature gradient in the cell and to initiate circulation for the aqueous fluid. Bromine concentrations were measured in-situ with X-ray fluorescence in the basaltic melts, glasses, and in the fluid. From the results we calculated partition coefficients of $D^{Br}_{fluid/melt} = 1.19$ to 3.92 in the range of 0.4 to 1 GPa for aqueous fluids. Experiments with neon as the surrounding fluid ($D^{Br}_{fluid/melt} = 0.38 \pm 0.01$ at 1.1 GPa) suggest that Br-release from a basalt into volatiles that have no bonding affinity with Br is weak. This should be the case for dry intra-plate volcanic eruptions. From the experimentally gained partition coefficients and from global Br concentration values in melt inclusions of arc magmas, we calculated an annual global Br flux of 23.5–72.9 $\times$ 10^9 g/y.

1. Introduction

Halogens are very reactive chemicals and play a significant role as volatile elements in geodynamic processes. In crustal hydrothermal fluids (e.g., brines and molten salts), halogens are major agents for the metal transport and thus play a critical role in ore-forming processes (Aiuppa et al., 2009). Halogens are also important constituents of volcanic fumaroles and volcanic ejecta. Once released to the atmosphere halogens have an environmental impact and can e.g., contribute to ozone destruction (e.g., Daniel et al., 1999; Gerlach, 2004).

The heavy halogen bromine (Br) has a low abundance on Earth, but it is highly reactive and an important chemical agent in the atmosphere (Fehn, 2012). Besides plankton and burning biomass, volcanoes have been recognized as a significant (Gerlach, 2004) if not the controlling, (Pyle and Mather, 2009) contributor to the actual atmospheric Br content. Especially arc volcanoes release large amounts of Br gas compounds: The first detection of volcanic BrO has been recorded by Bobrowski et al. (2003) from the Soufrière Hills volcano (Montserrat). Since then, Br gas compounds have been reported in several case studies e.g., from Mt. Etna (Aiuppa et al., 2005; Pyle and Mather, 2009; Bobrowski and Giuffrida, 2012; Roberts et al., 2018) or Mt. Masaya (Witt et al., 2008).

Based on models from Etna's degassing measurements Br is estimated to be rather less abundant in basalts compared to e.g., chlorine (Cl) or sulfur (Bobrowski and Giuffrida, 2012). The Br concentrations range from μg/g to ng/g in volcanic rocks and in mantle rocks (Newsom, 1995). Yet, Br fluxes from arc volcanoes are estimated to be in the range of 5–15 $\times$ 10^9 g/y HBr per year (Aiuppa et al., 2005; Pyle and Mather, 2009; Webster et al., 2018; Cadoux et al., 2022). HBr is the dominant species of Br emitted from volcanoes (Roberts et al., 2018). Once in the stratosphere, Br is notably involved in the destruction of ozone as it reacts to form BrO and eventually BrO_x (Bobrowski et al., 2003). These

* Corresponding author at: Research School of Earth Sciences, Australian National University, Canberra, Australia.
E-mail addresses: tobias.gruetzner@wwu.de (T. Grützner), helene.bureau@upmc.fr (H. Bureau), eglantine.boulard@sorbonne-universite.fr (E. Boulard), pascal.munsch@irap.omp.eu (P. Munsch), nicolas.guignot@synchrotron-soleil.fr (N. Guignot), siebert@ipgp.fr (J. Siebert), yoann.guarnelli@sorbonne-universite.fr (Y. Guarnelli).

https://doi.org/10.1016/j.chemgeo.2023.121869
Received 22 June 2023; Received in revised form 22 November 2023; Accepted 26 November 2023
Available online 30 November 2023

conversions are significant: 1 ng/g of BrO can destroy about 10 ng/g of ozone per minute (Bobrowski et al., 2003). This is about 60 times more efficient (Sinnhuber et al., 2009) than the ozone destruction by Cl in this respect (Daniel et al., 1999; Gerlach, 2004; Gutmann et al., 2018 for review).

However, the deep cycling of Br, its behavior in magmas, and the transfer to the Earth's surface is poorly understood. There is scant data, but Br solubility has been shown to be very high in silica-rich systems (Bureau and Métrich, 2003; Bureau et al., 2010). Depending on the Br content in degassing magmas the annual volcanological Br flux to the atmosphere could be strongly underestimated, and therefore, the impact of Br on ozone destruction in the Earth's stratosphere as well.

So far, there are only a few experimental studies about Br partitioning between a silicate melt and a fluid. The pioneering study was conducted by Bureau et al. (2000) with an albitic melt composition at 200 MPa from which the authors calculated a partition coefficient between the aqueous fluid and the silicate melt of $D^{Br}_{fluid/melt} = 17.5 \pm 0.6$. Bureau et al. (2010) found smaller values with $D^{Br}_{fluid/melt}$ ranging from 2.18 to 9.2 ± 0.5 between aqueous fluids/saline fluids and a haplogranitic melt at higher pressures of 0.66 to 1.7 GPa. Using a similar haplogranitic melt, Louvel et al. (2020b) found values of $D^{Br}_{fluid/melt}$ between 2.0 ± 0.2 and 15.3 ± 2.0 at pressures of 0.2 to 1.7 GPa. Louvel and coworkers did not find a clear correlation with pressure or temperature in their results. The experiments from Bureau et al. (2010) and Louvel et al. (2020b) were measured in-situ and give a good insight into Br partitioning between melt and fluid, but they were conducted in compositionally simplified systems (e.g., Fe-free melts) and rather aimed to study more evolved melts like sediment melt composition with higher SiO_2 content.

Cadoux et al. (2018) conducted partitioning experiments for Br between fluid and a wider range of arc-related rocks: natural basalt, andesite, and rhyodacite at 100–200 MPa. They calculated $D^{Br}_{fluid/melt}$ of 4.6 to 27.9 with basalt at the lower end and rhyodacite at the upper end of their partition coefficients. Experiments from Cadoux et al. (2018) show generally higher partition coefficients than the results from Bureau et al. (2010) which could describe the impact of the lower pressure used by Cadoux et al. (2018).

Not much is known about the effect of the different cations on $D^{Br}_{fluid/melt}$. Bromine concentrations vary in water-saturated silicic melts with (Na + K)/Al molar ratio and reach a minimum at (Na + K)/Al = 1 (Bureau and Métrich, 2003). A comparison to Cl advocates for the presence of alkalis to increase Br solubility: Cl solubility in melts is controlled by the abundances of several elements like Mg, Ca, Fe, Na, K, Al, Li, Rb, Cs, Ti, F, and P (Webster and de Vivo, 2002; Webster et al., 1999). Cochain et al. (2015) demonstrate that alkalis and especially Na can retain Br in a silicate melt while it degasses more efficiently from hydrous melts. Louvel et al. (2020b) find that Br prefers Na over OH in silicate glasses, where it is incorporated in a salt-like structure, like NaBr. Louvel et al. (2020a) show that Br bonds with network modifiers in granitic melts but does not find any affinity to prefer Na^+ over e.g., K^+ or Ca^{2+} if all three are present.

In this study we present new Br degassing experiments from a natural arc-related basalt into an aqueous fluid and into neon. The experiments were conducted over a pressure range from 0.4 to 1.7 GPa in the closed system of a diamond anvil cell which has already been used successfully by Bureau et al. (2010), to study Br. Partitioning of Br between the basalt and the surrounding fluid can be calculated from both in-situ measurements on melts and on quenched glass.

2. Methods

2.1. Diamond anvil cell setup

Two series of experiments were performed as hydrous and neon experiments which refer to the pressure media water and neon, respectively. As the basalt glass with about 2 wt% of water was also used in the *neon* runs, these runs were not completely dry sensu stricto (for a detailed description of the starting material see further below). The water-basalt-partitioning experiments (hydrous) were conducted in externally heated hydrothermal diamond anvil cells (HDAC) of either the Basset type (e.g., Bassett, 2003) or a modified Basset type with pressure-driving membranes (Munsch et al., 2015). Similar setups have been used successfully in former studies on heavy halogen behavior in silicate glass and hydrothermal fluids (e.g., Bureau et al., 2010, 2016; Louvel et al., 2020b). All HDAC are equipped with 2 mm thick diamonds with large culets of 1 mm diameter. The sample chamber is compressed between two diamonds and has a diameter of 500 μm which is drilled as a hole into a Re gasket of either 100 μm or 200 μm initial thickness. The aqueous fluid serves as a pressure medium within the sample chamber. Both diamonds are mounted on tungsten carbide (WC) seats. A molybdenum wire coiled around each WC seat serves as external heater. The temperature can be measured with K-type thermocouples that are glued with cement to each of the diamond anvils. The temperature offset between the thermocouple position and the sample chamber has been calibrated at ambient pressure against the melting temperature of pure sulfur (112.8 °C), $NaNO_3$ (308 °C), CsCl (645 °C), and NaCl (801 °C). To avoid oxidation of the diamonds while using the external heaters, the HDAC are connected to a gas supply system and can be flooded with a reducing gas mix like Ar—H_2 (4 vol%).

For neon experiments we used an inert gas as pressure medium. We performed neon-basalt partitioning experiments which were conducted in modified Chervin-type diamond anvil cells (Chervin et al., 1995). These DAC are equipped with a pressure driving membrane like the Basset-type HDAC but do not have an external heating system. Chervin type cells (CDAC) can be installed into the gas loading system e.g., at the Institut de Minéralogie, de Physique des Matériaux et de Cosmochimie (IMPMC – Sorbonne Université Paris) where we loaded the sample chamber with neon gas instead of water as a pressure medium (Couzinet et al., 2003). Neon has a density like air. It was loaded with an initial pressure of about 0.5 GPa into the DAC. At this pressure neon behaves as a (supercritical) fluid. The CDAC are equipped with the same type of diamonds, rhenium gaskets, and the same sample chamber dimensions that were used for the HDAC. All used DAC types in this study allow observation of the experiment and laser heating along the pressure axis through the diamond anvils.

2.2. Experimental runs, heating, and temperature determination

For each experiment the sample chambers were filled with 1–3 larger pieces of basalt glass (about 30–50 vol%, 55–75 wt% respectively), and 50–70 vol% of either water or neon gas (+ small flakes of gold + ruby spheres in neon experiments for pressure determination). The samples were compressed to about 1–2 GPa before the run. To heat the basalt glass to its liquid state, we used two YAG laser that can be focused on the sample from both sides of the pressure axis – one through each diamond. YAG laser can be used as the iron content of the basalt glass starting material (8.45 wt%) is high enough to provide the required absorption. During the heating the melt was analyzed with Synchrotron X-Ray Diffraction (SXRD) to test for the presence of crystals in the melt. If crystals (olivine or pyroxene) were present, the laser temperature was increased stepwise until all the crystals were melted. The laser heating temperature ranged from 1725 to 2167 °C for the neon experiments. It could not be measured for hydrous experiments but by monitoring the absence of crystals by XRD we could ensure to stay above the liquidus. This would be a temperature of 1300 to 1400 °C for the hydrous basalt. Experimental conditions are listed in Table 1.

For the hydrous experiments heating cycles (usually 5 min at the peak temperature) and decompression paths were varied between each run: During experiment LN11 and LN22 the basalt glass was heated with the laser to its liquid state and quenched afterwards by shutting off the laser. Br concentrations were then analyzed in the glass and in the fluid. This heating-quenching-analyzing cycle was repeated several times with

Table 1
Experimental runs. Bromine was analyzed with synchrotron x-ray fluorescence. Uncertainties on the bromine concentrations are of 10% relative. RT = room temperature; nd = not detectable. The volume of the fluid fraction was estimated from sense of proportion and ranges from 25 to 45 wt%.

Experiment-Run	Pressure (GPa)	Heating cycles	Laser Temperature (°C)	Pressure medium/fluid	Bromine concentration (μg/g)			$D^{Br}_{fluid/melt}$
					melt	glass	fluid	
hydrous experiments								
Cpo2	< 1.1	0	RT	water		11160[a]	48[a]	
	< 1.1		RT	water			26[a]	
	< 1.1	1[b]	nd[g]	water		1070	2029	1.9
LN22	< 1.1	0	RT	water		11120[a]	18[a]	
	< 1.1	1[b]	nd[g]	water		2739	7455	2.72
	< 1.1	2[b]	nd[g]	water		3267	6864	2.10
	< 1.1	3[b]	nd[g]	water		2124	7027	3.31
	0.4[f]	4[b]	nd[g]	water		3282	7178	2.19
Cpo3	< 1.1	0	RT	water		12440[a]	79[a]	
	< 1.1	1[b]	nd[g]	water			2563	
	< 1.1		nd[g]	water			2130	
	< 1.1		nd[g]	water			2498	
	< 1.1		RT	water		1990	2370	1.19
LN11	< 1.1	0	RT	water		12610[a]	−/80[a,d]	
	< 1.1	1	nd[g]	water		12,410	3462/358[d]	0.28/0.03[e]
	< 1.1	2	nd[g]	water		1062	4161/326[d]	3.92/0.31[e]
	< 1.1	3	nd[g]	water		1438	4783/267[d]	3.33/0.19[e]
	< 1.1	4	nd[g]	water		1752	5784/226[d]	3.30/0.13[e]
	0.53[f]	5	nd[g]	water		1545	5337/565[d]	3.45/0.37[e]
neon experiments								
Mar1	1.7	0	RT	Neon		10620[a]	209[a]	
	1.7	1	1875	Neon	14,640			
	1.7		1810	Neon	15,350			
	1.7		≈ 1800	Neon	15,200			
	1.7		≈ 1800	Neon	14,720			
	1.7		≈ 1800	Neon	16,430			
Hak1	1.7	0	RT	Neon		16,760	6212	0.37
	1.1		RT	Neon		10019[a]	1062[a]	
		1	2005	Neon	32,046			
			2120	Neon	45,065			
	1.1	2	RT	Neon		11,019	4153	0.38
			nd	Neon	43,095			
			2167	Neon	11,256			
	1.1	3	RT	Neon		10,148	3985	0.39
			2057	Neon	10,623			
			2057	Neon	9864			
Hak2	< 1.1	0	RT	Neon		10,128	208	0.02
	≥ 1.4		RT	Neon[c]		10138[a]	11760[a]	1.16
	≥ 1.4	1	≈ 1725	Neon[c]		4333	7087	1.64
	≥ 1.4	2	≈ 1725	Neon[c]		4398	8060	1.83
	1.4	3	≈ 1725	Neon[c]		5974	10,314	1.73

[a] Initial bromine concentration measurements were done in a compressed cell at ambient temperature before the first heating.
[b] External heating kept the temperature at 235–265 °C when the las was shut off to enable fluid circulation.
[c] The Neon fluid became enriched in water that was first released from the basalt glass in run Hak1–3 and together recompressed for Hak2 runs.
[d] Two separate fluid analyses were conducted: '*next to the melted glass*'/'*200* μm *away from the glass*'.
[e] Partition coefficients calculated for the fluid '*next to the melted glass*'/'*200 μm away from the glass*'.
[f] Determined by ice-water transition from Nitrogen cooling after the experiment.
[g] Laser temperature was above the liquidus temperature for hydrous basalt (> 1300 °C). The absence of crystals was monitored with SXRD.

a stepwise pressure release in the sample chamber after each cycle to test for pressure effects on Br partitioning (c.f. Bureau et al., 2010, 2016; Leroy et al., 2019) and to reach chemical equilibrium (see further below in the Results section for detailed description). Experiment Cpo2 had only one heating-quenching cycle. For experiment Cpo3 the laser heating was not switched off for the decompression steps, but instead it was constantly keeping the basalt above the liquidus. The Br concentration was analyzed in the fluid of Cpo3 while the laser was switched on and the basalt was still molten. During run Cpo2, Cpo3 and LN22 the external heaters were additionally heating the sample chamber of the HDAC for the entire run (244 °C, 265 °C and 235 °C respectively). This minimized the temperature gradient caused by the heating laser and induced a better circulation and homogenization of the fluid. To test this effect the external heating system was shut off in experiment LN11: the fluid was not heated externally, and Br was measured at two fixed positions (Fig. 1a): The first spot is next to the melted and quenched basalt. The second spot is about 200–300 μm away at the rim of the sample chamber (as it was also the case for all other hydrous experiments). During the laser heating the temperature of the HDAC measured at the thermocouples increased to 260–280 °C. This was independent from the external heating system being switched on (LN22, Cpo3) or off (LN11).

The neon experiments Hak1 and Hak2 were performed in CDAC with neon as the pressure medium and with similar heating cycles as described above for LN11 and LN22: after crossing the basalt glass transition with the laser and keeping the laser for 5 min at the peak temperature, the laser was shut off, Br concentrations were analyzed in

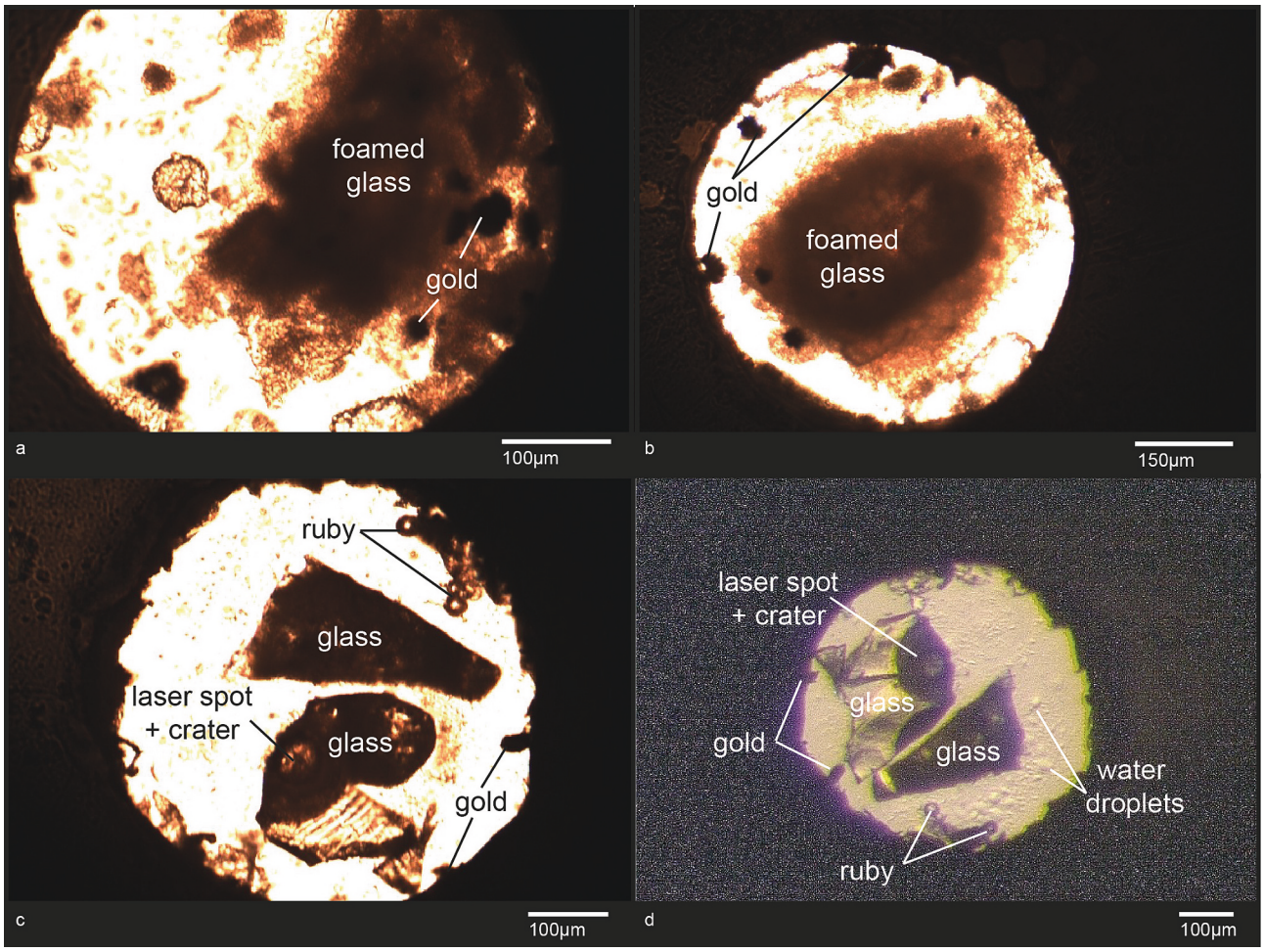

Fig. 1. Optical microscope images of sample chambers and experimental samples LN11, LN22, Hak2 and Hak1. a) LN1: Two spots of measurement for the aqueous fluid were chosen. One close to the melted glass and one as far away as possible within the sample chamber. b) LN22: like in a) the basalt glass shows a foam-like texture after treatment with the heating laser. c) Hak2: In contrast to a) and b) laser heated glass in coexistence with neon retains its glassy texture. d) Hak1: During heating cycle 3 and ongoing decompression of the cell water droplets could be observed in the sample chamber.

the glass and in the fluid (neon), and the pressure was decreased before starting the next heating cycle again. During the experiment of Hak1 Br was additionally measured twice in the basaltic melt during each heating cycles. After the conduction of run Hak1 the cell was kept closed and directly re-compressed to 1.4 GPa to conduct run Hak2 on the same loading. Mar1 had only one long heating cycle: The laser was not switched off during the decompression steps and for each decompression step in Mar1 Br concentration was measured in the liquid basalt (600 s. for each analysis).

2.3. Pressure determination

2.3.1. Setup

Pressure determination in the loaded and compressed DAC was conducted in several ways using (1) ruby fluorescence, (2) gold SXRD, and the (3) water-ice phase transition.

(1) For the neon experiments small ruby spheres were added during loading into the sample chamber of the CDAC. The pressure was measured at room temperature before and after the run with the fluorescence method at the IMPMC and at Soleil. The fluorescence wavelength shift of ruby is a commonly used pressure sensor for DAC experiments (e.g., Chervin et al., 2001; Shen et al., 2020). Ruby fluorescence is commonly used as a pressure sensor in DAC experiments, but it was not added to the HDAC experiments as it dissolves quickly in the heated aqueous fluid, possibly causing chemical pollution.

(2) In all experiments small gold particles were added into the sample chambers to determine the pressure in-situ with SXRD during the run. Gold was measured usually after quenching of the laser heating cycle. The SXRD analyses were processed with DIOPTAS (Prescher and Prakapenka, 2015) and the GSAS-II (Toby and Von Dreele, 2013) software. The pressure shift from the equation of state (EOS) for gold was calculated after Dorogokpets and Dewaele (2007) in the web application http://kantor.50webs.com/diffraction.htm. Unlike ruby, the gold flakes do not dissolve in hydrous experiments. In the neon experiments, the addition of gold allowed us to compare it to the ruby fluorescence pressures.

(3) For the hydrous experiments LN11 and LN22 the pressure was determined additionally after the run using the EOS for water and following the method described by Bassett et al. (1993). The water-ice phase transition was used to calculate the fluid density in the sample chamber: this was done after the experiment (the HDAC were kept closed) and not during the experimental session at Soleil. The sample chamber of the HDAC was cooled down with liquid nitrogen and the temperature of the phase transition between water and ice VI in the aqueous fluid was measured with the attached thermocouples. Pressures were then calculated from the EOS for the water-ice transition (Wagner and Pruß, 2002).

This is feasible as the use of the EOS of water in silicate-water systems has been validated by Munsch et al. (2015). Table 2 lists all calculated pressures from gold, water-ice transition, and ruby.

2.3.2. Challenges in pressure determination

Pressure determination in the HDAC is challenging and was often not satisfying during for the conducted runs. The sample chamber is a closed system during the experiment and once it has been compressed, the pressure inside remains constant if the cell does not leak or the pressure is altered – intentionally or by damaging. While the sample is heated the pressure increases inside the sample chamber due to thermal pressure, but it decreases again after quenching/during cooling of the sample. Therefore, ruby fluorescence in neon experiments shows the same pressure before and after the experiment (at room temperature) and confirms that the system remained close (Table 2). To prevent all parts of the loaded cell from damage suffering in hydrous experiments, the nitrogen cooling for pressure determination with the EOS of the water-ice transition was only applied after cessation of the experiment while the HDAC were kept closed. During sample loading of the hydrous experiments no high-pressure polymorphs of ice were observed in any of the loaded sample chambers at room temperature. Thus, none of the HDAC samples exceeded pressures of 1.1 GPa during the pre-experiment compression (c.f. Wagner and Pruß, 2002). The pressure determination from the water EOS is precise and reliable only for the last heating cycles performed in the HDAC. Respectively, the limit $P < 1.1$ GPa is proposed for the first heating cycles of each experiment (Table 1).

Table 2
Experimental pressures calculated from the equation of state (EOS) of water-ice VI transition, ruby fluorescence, and EOS of gold.

Experiment-Run	Heating cycles	Pressure (GPa)		
		water-ice VI transition	ruby	gold
Cpo2	0	< 1.1[a]		2.6[b]
	1	–		2.1
LN22	0	< 1.1[a]		2.1[b]
	1	–		–
	2	–		–
	3	–		–
	4	0.4[c]		2.0[c]
Cpo3	0	< 1.1[b]		1.6[b]
	1	–		–
		–		–
		–		–
		< 1.1		2.1
LN11	0	< 1.1[b]		1.9[b]
	1	< 1.1		–
	2	< 1.1		0.8
	3	< 1.1		0.9
	4	< 1.1		1.2
	5	0.53		2.0
Mar1	0		1.7[b,c]	2.7[b,c]
	1		1.7	–
			1.7	–
			1.7	–
			1.7	–
			1.7	–
			1.7[c]	3.2[c]
Hak1	0		1.1[b,c]	3.3[b,c,d]
	1		1.1	–
	2		1.1	–
	3		< 1.1	3.1[d]
Hak2	0		1.4[b]	–
	1		≥ 1.4	2.8
	2		≥ 1.4	2.4
	3		1.4[c]	1.9[c]

[a] Water-ice transition measurements were conducted after the experiment and after the cell cooled down to room temperature.
[b] Initial pressure measurements were done in a compressed cell at ambient temperature before the first heating.
[c] Pressure values are used for the method correlation in Fig. 2.
[d] Diffraction peaks could be also neon at 1.2 GPa.

Most pressures calculated from the EOS for gold do not agree well with the other two methods (Table 2). The pressures measured with gold are in average about 1.2 GPa higher than the pressures determined with water-ice transition or ruby. The difference between gold and both alternative methods show a moderate positive correlation of $r = 0.69$ (Fig. 2), with −1 or 1 for an excellent correlation and 0 for no correlation. However, the trend in Fig. 2 would be expected to match with $m = 1$ (dashed line), as all working pressure calculation methods should give the same results within an error, or it should describe a nonlinear approach to 1 on a larger pressure scale. We used only data points where the pressure was measured under the same conditions with two different methods for Fig. 2. The dataset is small, and the range of pressure is limited to <1.7 GPa (ruby) which lies in the nature of the experiments of this study. A nonlinear approach towards the dashed line ($m = 1$) can be expected for pressures >2 GPa, but at lower pressures the EOS of gold shows a clear shift towards higher pressures (Fig. 2) and cause probably pressure overestimation.

Pressure values calculated from gold show further unexpected behavior during each experiment, as for several runs the pressure seem to remain elevated after the last quenching – relative to the first measured pressure before the start of the experiment. This is not in agreement with ruby fluorescence. Moreover, in experiment LN11 the pressure seems to drop during the laser heating from 1.9 GPa to 0.8–1.2 GPa for the first four heating cycles but seem to increase to 2.0 GPa after the last heating cycle (Table 2). A closure (volume change) of the sample chamber could not be observed.

We argue therefore that pressure calculations from the EOS of gold are unreliable for the applied pressure range of this study (< 2 GPa). Pressure data in this range calculated from gold XRD are rather estimates and must be handled with care.

2.4. Starting material composition

For the starting material, we used a natural island arc basalt from the Soufriere volcano on St Vincent Island, Lesser Antilles arc (STV301 glass Pichavant et al., 2002) that was enriched in Br and water: The basalt was

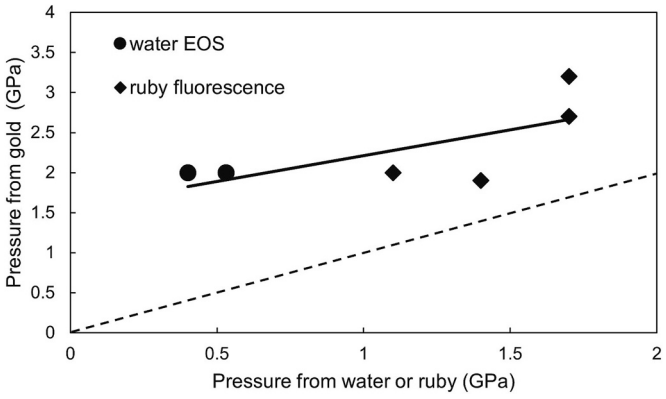

Fig. 2. Pressures in the DAC sample chamber calculated from the EOS for gold vs. pressures calculated from the EOS for water or from ruby fluorescence. The linear trend (black line) shifts from the expected trend (dashed line) between the applied methods. (For interpretation of the references to colour in this figure legend, the reader is referred to the web version of this article.)

grounded into a fine grain powder to which 3 wt% of NaBr and 2 wt% of H_2O were added. We melted the powder in a Boyd & England-type piston cylinder apparatus (Boyd and England, 1960) at the Institut de Physique du Globe de Paris (IPGP) to obtain a glass of this hydrous, Br-bearing basaltic mixture. Synthesis conditions for our starting glass were 1.1 GPa, 1300 °C and 30 min run duration. A sealed Au—Pd capsule prevented major iron loss. Small pieces of the Br-bearing hydrous glass were used for the in-situ experiments. For the aqueous fluid we used distilled water.

The synthesized basaltic starting material is texturally homogenous. We used an optical microscope first, and an electron microscope (FEG Zeiss Ultra55) at the IMPMC, Sorbonne Université Paris to check the glass for impurities. The glass looks homogenous and no crystals, gas- or water bubbles could be found. Major and minor elements were analyzed with a JEOL 8530F Plus Electron Probe Microanalyser (EPMA) at the Centre for Advanced Microscopy, ANU in Canberra, Australia and confirmed that the basalt glass is also chemically homogenous. The composition of the starting glass can be found in Table 3. The Br concentration is about 1.1 ± 0.1 wt% (with EPMA) and was confirmed with Synchrotron X-ray fluorescence (SXRF) in the basalt glass before each experiment.

2.5. In-situ analysis of Br concentrations

Bromine concentration in basalt glass, aqueous fluid, and neon were measured quantitatively by SXRF in situ analysis in the diamond anvil cells (DAC) at the SOLEIL Synchrotron on the PSICHÉ beamline. We used a monochromatic beam of 33 keV that was masked by a pinhole of 50 µm in diameter and focused at 12 × 10 µm^2. For each experiment the DAC was positioned perpendicular to the beam. Both SXRF and SXRD were detected in transmission geometry. SXRF was detected by a SDD detector which was placed at 24° relative to the beam transmitted through the DAC. Counting times were usually set to 600 s.

SXRF analyses were calibrated on a 240 µm thick piece of the NIST silicate glass certified reference material SRM 610 (e.g., Rocholl et al., 1997). The Br content in NIST 610 is not quantified but NIST 610 is calibrated for multi elemental analyses on glasses and covers a broad range of elements including elements with Kα peak energies close to the Kα peak of Br (11.9 keV) e.g., Se (11.2 keV), As (10.5 keV) or Sr (14.1 keV). The volcanic glass V1 (Mosbah et al., 1995) was measured additionally as standard glasses, as well as a piece of the Br-H_2O-doped starting glass (BaM024). To test for any effects of DAC setup on SXRF measurements NIST 610 was also placed in the DAC at ambient pressure and temperature. No effects could be found between the different NIST analyses. All glasses show good agreements for their element concentrations in the energy range of Br (Table 4). During the experiments basalt glass analyses were conducted in the center of the heated region (the crater-like texture in neon experiments). The detection limit is typically in the range of of 1–10 µg/g, which is in good agreement with similar studies (e.g. Louvel et al., 2020a) and with what can be expected for elements of a similar mass (Rousseau, 2021).

Table 3
Major and minor element composition of the basaltic glass stating material in wt% measured with electron microprobe analysis. Uncertainties (1 s.d.) are given in parentheses showing the first significant digit.

SiO_2	44.9(2)
TiO_2	1.08(3)
Al_2O_3	14.5(1)
Cr_2O_3	0.09(2)
FeO	8.45(7)
MnO	0.15(2)
NiO	0.03(2)
MgO	11.8(1)
CaO	10.66(6)
Na_2O	2.61(6)
K_2O	0.50(1)
P_2O_5	0.10(2)
Total	95.6(3)

Table 4
Bromine concentration in the starting glass measured by synchrotron x-ray fluorescence and electron microprobe analysis. Uncertainties on the bromine concentrations are of 10% relative.

Sample	Bromine (µg/g)
BaM024	10,812
Cpo2–0	11,160
LN22–0	11,120
Cpo3–0	12,440
LN11–0	12,610
Mar1–0	10,620
Hak1–0	10,019
Mean	11,254
SD	726

The gaskets of each experiment were recovered, and their thickness was measured after the run to calculate the change in the set-up geometry of the SXRF analyses during the experiments. To quantify the Br concentration in the basaltic glass, the aqueous fluid, or in neon all obtained SXRF spectra from standards and experiments were processed by using the PyMCA software (Solé et al., 2007). We compared the Br concentration of the starting material with the calculated values from PyMCA for the first measurement at room temperature for each experiment. If both values were not in agreement, we assumed that the basalt glass was not touching both diamonds. The initial thickness of the glass was then calculated using PyMCA by adding a water/neon layer to fit the calculated Br concentration with the value from the starting material. For matrix corrections we assumed a 2.9 g/cm^3 for basalt, 1–1.2 g/cm^3 for water and 0.5 g/cm^3 for supercritical Neon.

3. Results

3.1. Textural observations

Textural changes of the basalt glass were observed after quenching the experiment. In hydrous experiments the glass has a spongy or foam-like texture after the ultra-fast quenching induced by the laser turn off which causes very fast local water exsolution (Fig. 1a-b). This transformation into a foam affected a volume that is much larger than the original laser heating spot and is seen at the rim of the glass piece. It shows therefore that almost the whole glassy volume is melted during the heating. These textures have not been observed in studies with haplogranite where the external heating is strong enough to melt the entire glass in the sample chamber of the HDAC and when temperatures decrease slowly (Bureau et al., 2010; Louvel et al., 2020b). The spongy textures were not found in neon runs. As a study from Balcone-Boissard et al. (2020) shows, bromine diffusion in related melts is much lower than that of H_2O. External heating was added to lower the temperature gradient and to support the homogenization of the hydrothermal fluid in several experiments, but temperatures were not high enough to melt the entire piece of glass or even reach full miscibility between melt and fluid. Nevertheless, experiments like LN11 and LN22 for water show reproducible results and equilibration between the Br concentration in the glass and in the surrounding fluid within their runs.

In neon experiments the melting spots of the laser are clearly visible but the glass around the laser appears to be texturally unharmed (Fig. 1c-d). The temperature gradient is larger than in the hydrous experiments because no external heating was applied to the CDAC. However, the basalt glass shows no strong reaction with neon.

All experimental results are listed in Table 1.

3.2. Hydrous experiments

3.2.1. Run Cpo2

Run Cpo2 shows Br loss to the surrounding aqueous fluid: Br concentration before the first heating is 11,160 μg/g in the glass and 26–48 μg/g in the fluid. For this run the temperature of the laser could not be measured precisely. After quenching the concentration changes to 1070 μg/g in the glass and 2029 μg/g in the fluid (Fig. 3a). A partition coefficient of $D^{Br}_{fluid/glass} = 1.9$ was calculated. The pressure could not be determined precisely, but according to the stability of water and ice VI at room temperature the pressure in the loaded cell is <1.1 GPa (Wagner and Pruß, 2002). Gold SXRD gave a pressure range of 2.6 GPa before the heating and 2.1 GPa after the heating.

3.2.2. Run LN22

In run LN22 Br concentration before the first heating is 11,120 μg/g in the glass and 18 μg/g in the aqueous fluid. The laser temperature could only be estimated but SXRD confirmed that it was above the solidus of the hydrous basalt. After quenching the concentrations change to 2124–3282 μg/g in the glass and 6864–7455 μg/g in the fluid for all four cycles (Fig. 3b). A range of $D^{Br}_{fluid/glass} = 2.10–3.31$ was calculated. The pressure range is between 0.4 and 1.1 GPa during the experiment according to water and decreased slightly from 2.1 GPa to 2.0 GPa according to gold.

Br concentration in water and basalt reach a plateau after the first heating cycle (Fig. 3b). This is a good indicator that chemical equilibrium has been reached in the experiment.

3.2.3. Run Cpo3

In run Cpo3 Br concentration is 12,440 μg/g in the glass and 79 μg/g in the aqueous fluid before the heating. While the laser keeps the basalt liquid, the Br concentration in the fluid ranges from 2130 to 2563 μg/g. After quenching the concentrations is 1990 μg/g in the glass and 2370 μg/g in the fluid (Fig. 3c). A value of $D^{Br}_{fluid/glass} = 1.19$ can be calculated. According to run Cpo3 there are no notable changes in Br concentration before and after quenching the glass. As for run Cpo2 the pressure is <1.1 GPa according to water but increases from 1.6 GPa to 2.1 GPa according to gold.

3.2.4. Run LN11

Bromine concentration before the first heating is 12,610 μg/g in the glass and 80 μg/g in the aqueous fluid. After the first quenching the Br concentration remains high in the glass (12,410 μg/g) but becomes slightly lower after heating-quenching cycle 2–5 (1062–1752 μg/g). In

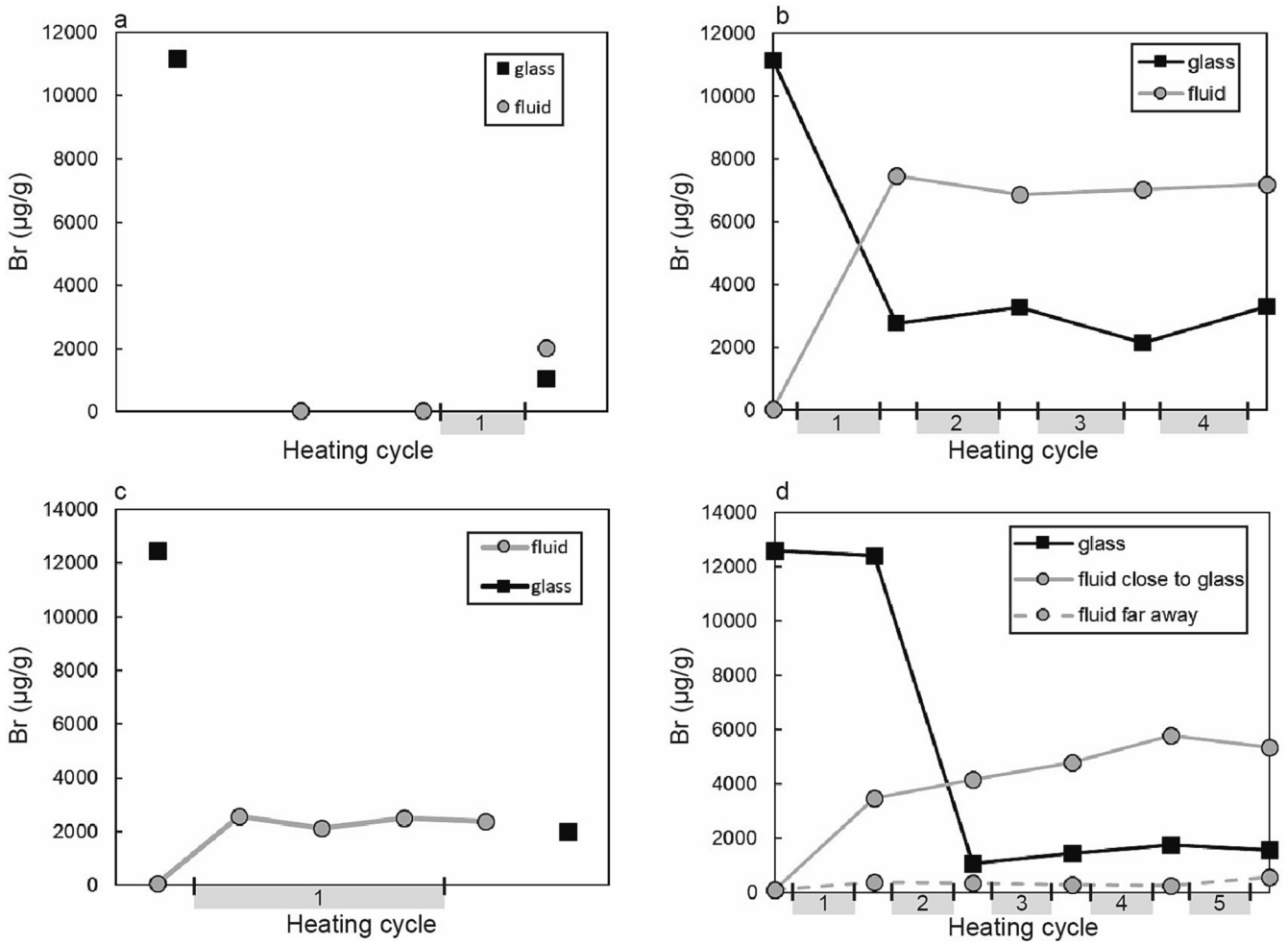

Fig. 3. Bromine concentration versus time/heating cycles in hydrous experiments. During each heating cycle step the basalt glass was melted, quenched, and analyzed again. a) Cpo2: Already the first heating cycle reduces the Br concentration in the basalt dramatically. b) LN22: Bromine concentrations in the basalt glass and in the aqueous fluid equilibrate quickly after quenching the first heating cycle and remain on relatively constant levels. The plateau of the curve is a good indicator for chemical equilibrium. c) Cpo3: Bromine concentration in the aqueous fluid equilibrates quickly and remains constant after quenching. d) LN11: Without the usage of external heating the concentration of bromine in the aqueous fluid is not homogenized and shows a distinct difference between the concentrations analyzed close to the melted glass and further away.

the fluid, measurements close to the melted glass show that the Br concentration ranges from the first to the fifth quenching between 3462 and 5784 μg/g. Further away from the glass, the values range from 226 to 565 μg/g (Fig. 3d). While Br shows a concentration gradient the partitioning between fluid and glass remains relatively constant in cycle 2–5 with $D^{Br}_{fluid/glass} = 3.30$ to 3.92 close to the glass and $D^{Br}_{fluid/glass} = 0.13$ to 0.37 at the rim of the sample chamber. The pressure range is between 0.53 and 1.1 GPa calculated from water EOS and varies between 0.8 and 2.0 GPa calculated from the EOS for gold.

3.3. Neon experiments

3.3.1. Run Mar1

In run Mar1 bromine concentration before the first heating is 10,620 μg/g in the glass and 209 μg/g in the neon. During laser heating the concentration increases slightly from 14,640 to 16,430 μg/g in the melt. It remains high (16,430 μg/g) in the quenched glass and increased in the neon to 16,212 μg/g (Fig. 4a). A partition coefficient of $D^{Br}_{neon/glass} = 0.37$ can be calculated from the Br values in the fluid and in the glass. The pressure is 1.7 GPa according to ruby fluorescence and increases from 2.7 to 3.2 GPa according to the EOS of gold. We assume that the observed change in concentration comes from slight variation in the glass thickness between the different heating cycles. The melt can become spherical and might have extended further in the direction of the beam within the sample chamber. While Br concentration increased during the ongoing melting the calculated partitioning between glass and fluid is in good agreement with the Hak1 run (see below).

3.3.2. Run Hak1

In run Hak1 bromine concentration before the first heating is 10,019 μg/g in the glass and 1062 μg/g in the neon. During the first heating cycle Br concentration ranges from 11,019 μg/g to 45,065 μg/g in the melt and in the quenched glass respectively. In the second and third heating cycles Br concentration remains lower in the melt and in the glass ranging from 9864 μg/g to 11,256 μg/g. In the neon the measured Br concentration increases to 4153 μg/g, 3985 μg/g, and 208 μg/g after each of the three quenching cycles. Currently, we cannot fully explain the high Br values in the melt for the first two heating cycles. Volume changes during the melting could explain the variations. However, in heating cycle 2 and 3 the Br values decrease and equilibrate with the values measured in the glass. The $D^{Br}_{neon/glass}$ values are 0.38, 0.39, and 0.02, respectively (Fig. 4b).

The pressure is 1.1 GPa after loading the cell measured with ruby fluorescence or 3.3 GPa with gold. At this pressure the diffraction peaks also overlap with neon at 1.2 GPa. Like in all other experiments with neon, the external pressure (1.1 GPa) is released stepwise between each heating-quenching cycle. After the last quenching small droplets of water could be observed as a third phase in the sample chamber (Fig. 1d; Fig. 5). This observation suggests a pressure < 1.1 GPa after the last quenching but will be discussed in more detail further below. The calculated pressure from gold is 3.1 GPa (1.2 GPa from neon) at the end of the experiment.

3.3.3. Run Hak2

For run Hak2 the closed cell with the sample Hak1 was recompressed

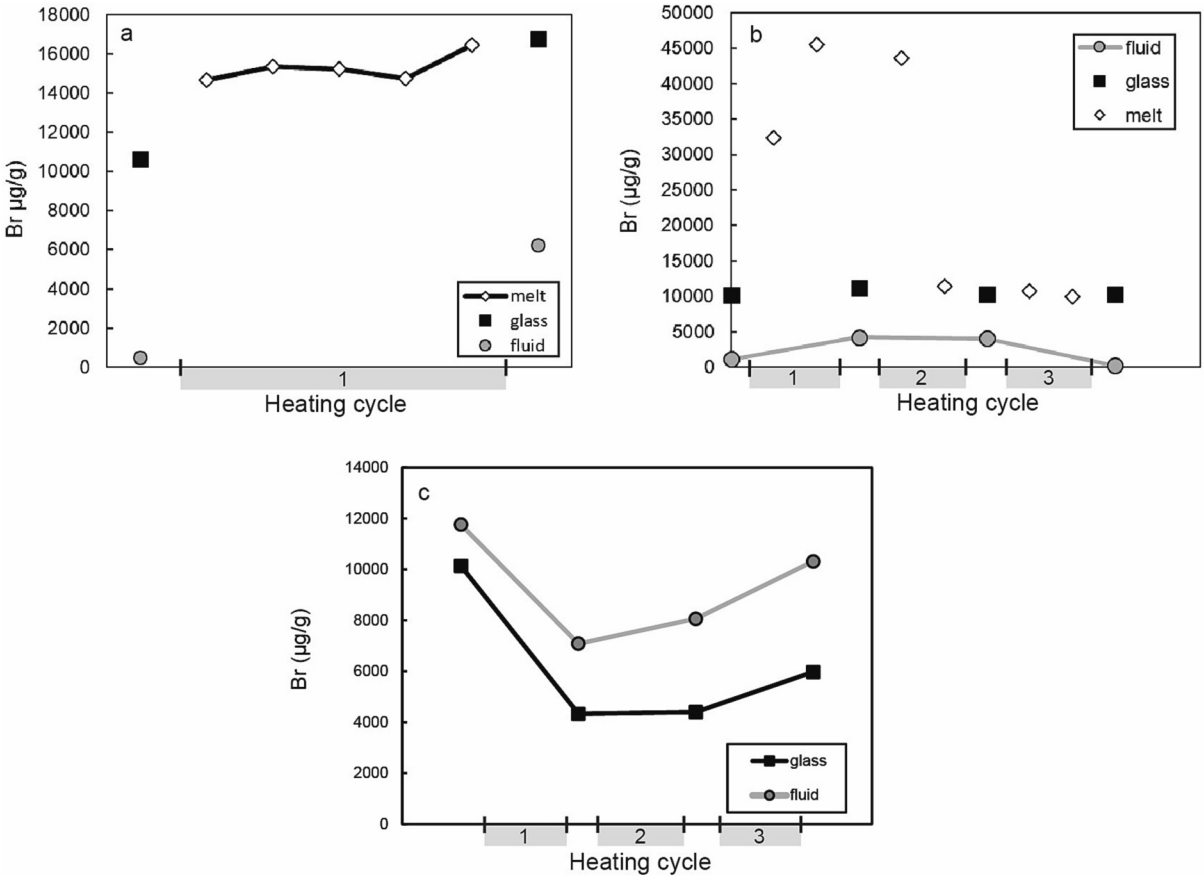

Fig. 4. Bromine concentration versus time/heating cycles in neon experiments. During each further heating cycle step the basalt glass was melted, quenched, and analyzed again. a) Mar1: Br concentrations remain high in the basalt glass and low in the neon. No changes in concentration appear between melt and glass. b) Hak1: The bromine concentrations measured in the neon remain lower than in the basalt glass. With ongoing decompression water is released from the hydrous basalt glass during the last heating cycle. We suspect bromine to partition into the released water while neon remains depleted in bromine. c) Hak2: Bromine concentration remain higher in the neon than in the basalt glass over all heating cycles.

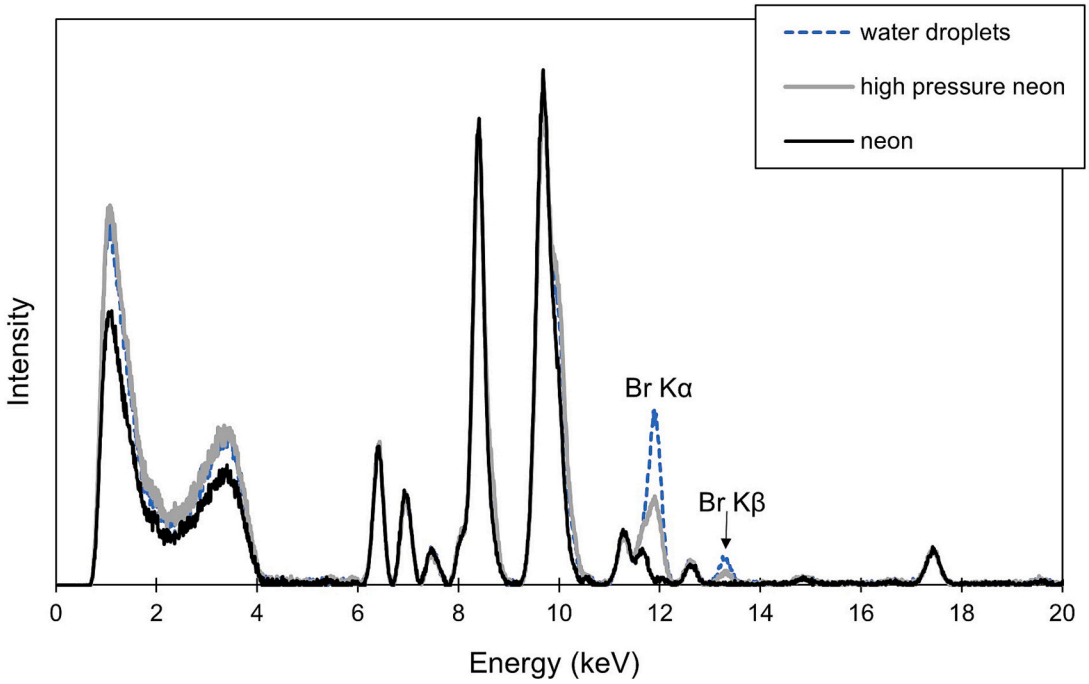

Fig. 5. Synchrotron X-ray fluorescence analysis of the pressure medium in run Hak1. High pressure neon was analyzed at heating cycle 2 while water was absent. The Br concentration in the HP neon is 4025 μg/g (grey). When the pressure was decreased in heating cycle 3 water bubbles released from the hydrous basalt could be observed in the neon (c.f. Fig. 1d). With the presence of water Br concentrated in the water bubbles (blue) and decreased in the neon down to 210 μg/g (black). (For interpretation of the references to colour in this figure legend, the reader is referred to the web version of this article.)

and used again for three heating-quenching cycles. Bromine concentration before the first heating is 10,138 μg/g in the glass and already high in the neon from the former run Hak1 with 11,760 μg/g. After quenching the concentrations range from 4333 to 5974 μg/g in the glass and 7087 to 10,314 μg/g in the fluid (Fig. 4c). A range of $D^{Br}_{fluid/glass}$ = 1.64–1.83 can be calculated. The ratio calculated from the Br concentrations before the first heating in this experimental run is $D^{Br}_{fluid/glass}$ = 1.16. The pressure determined with ruby spheres is 1.4 GPa before the first and after the last run. Gold pressure determination decreased from 2.8 GPa to 1.9 GPa.

4. Discussion

4.1. Bromine partitioning between basalt and aqueous fluids

The fluid-melt partitioning values from our experiments range from $D^{Br}_{fluid/melt}$ = 1.19 to 3.31 ± 0.6 – within the applied pressure and temperature range. These values overlap with findings from other studies but are slightly lower than the partition coefficients calculated by Bureau et al. (2010), Cadoux et al. (2018), and Louvel et al. (2020b). Partition coefficients between haplogranite and an aqueous fluid from Bureau et al. (2010) range from $D^{Br}_{fluid/melt}$ = 2.18 ± 0.4 to 15.3 ± 2 and values from Louvel et al. (2020b) range from $D^{Br}_{fluid/melt}$ = 2 ± 0.2 to 9.2 ± 1.8. Cadoux et al. (2018) found partition coefficients of $D^{Br}_{fluid/melt}$ = 3.8 to 5.2 from their experiments with basaltic composition and 8.6 to 27.9 from rhyodacite. With all calculated $D^{Br}_{fluid/melt} > 1$ the data from all four studies confirm that Br has a slight to strong affinity to partition from the melt into the aqueous fluid.

Partition coefficients from Cadoux et al. (2018) are generally higher than partition coefficients from the other three studies for comparable SiO_2 content (Fig. 6). One reason could be that Cadoux et al. (2018) did not conduct in-situ experiments and measured Br concentrations only in the quenched samples. In fact, the three other studies are all conducted and analyzed in-situ in HDAC – this study at least partially. Louvel et al. (2020b) argue that differences in the partition coefficients to Cadoux et al. (2018) might come from the quantification of Br by mass balance as it was used by Cadoux et al. (2018), or artifacts of the quench cooling that cause Br loss into the fluid. Louvel et al. (2020b) exclude their data point at 0.2 GPa, as they suspect uncertainties in the pressure determination below 0.5 GPa. Run Hak1 demonstrates that Br concentrations do not change significantly in our experiments in neon between basalt melt and quenched basalt glass (Fig. 4b), but it can be the case with water in externally heated DAC experiments up to 800–900 °C (e.g., Borchert et al., 2009; Bureau et al., 2010; Leroy et al., 2019). At these temperatures external heating increases the pressure in the sample chamber. Quenching the experiment can induce a pressure drop that affects the partitioning of elements like Sr, Rb, (Borchert et al., 2009) or Br (e.g., Bureau et al., 2010). Due to the selective heating of the laser, the pressure increase in the cell is small and fast diffusion during cooling plays a minor role in our experiments. Therefore, differences might also come from uncertainties in pressure determination or Br quantification in quenched samples.

Several trends for partition coefficients were described and suggested in existing studies on Br partitioning (e.g., Fig. 6): Bureau et al. (2010) found correlations of decreasing $D^{Br}_{fluid/melt}$ with increasing pressure and with increasing water content. Cadoux et al. (2018) found a correlation of decreasing $D^{Br}_{fluid/melt}$ with increasing temperature and with decreasing SiO_2 concentration within their data. This compositional effect of the melt was also described by Bureau and Métrich (2003) and Cochain et al. (2015). Louvel et al., 2020b found the variation in the partition coefficients to remain small over a large P-T range and do not find any clear trend. They propose that hydrous granite melts have a Br storage capacity similar to aqueous fluids. This makes sense as with increasing pressure and temperature, both fluid and melt tend to be equal before being miscible (Bureau and Keppler, 1999). This could buffer changing P-T conditions to some extent. Assuming a compositional trend, the basalt from Cadoux et al. (2018) has a higher $D^{Br}_{fluid/melt}$ than values from this study, which rather overlaps with the partition coefficients from the haplogranite of Bureau et al. (2010). The rhyodacite from Cadoux et al. (2018) has about the same amount of SiO_2 as the

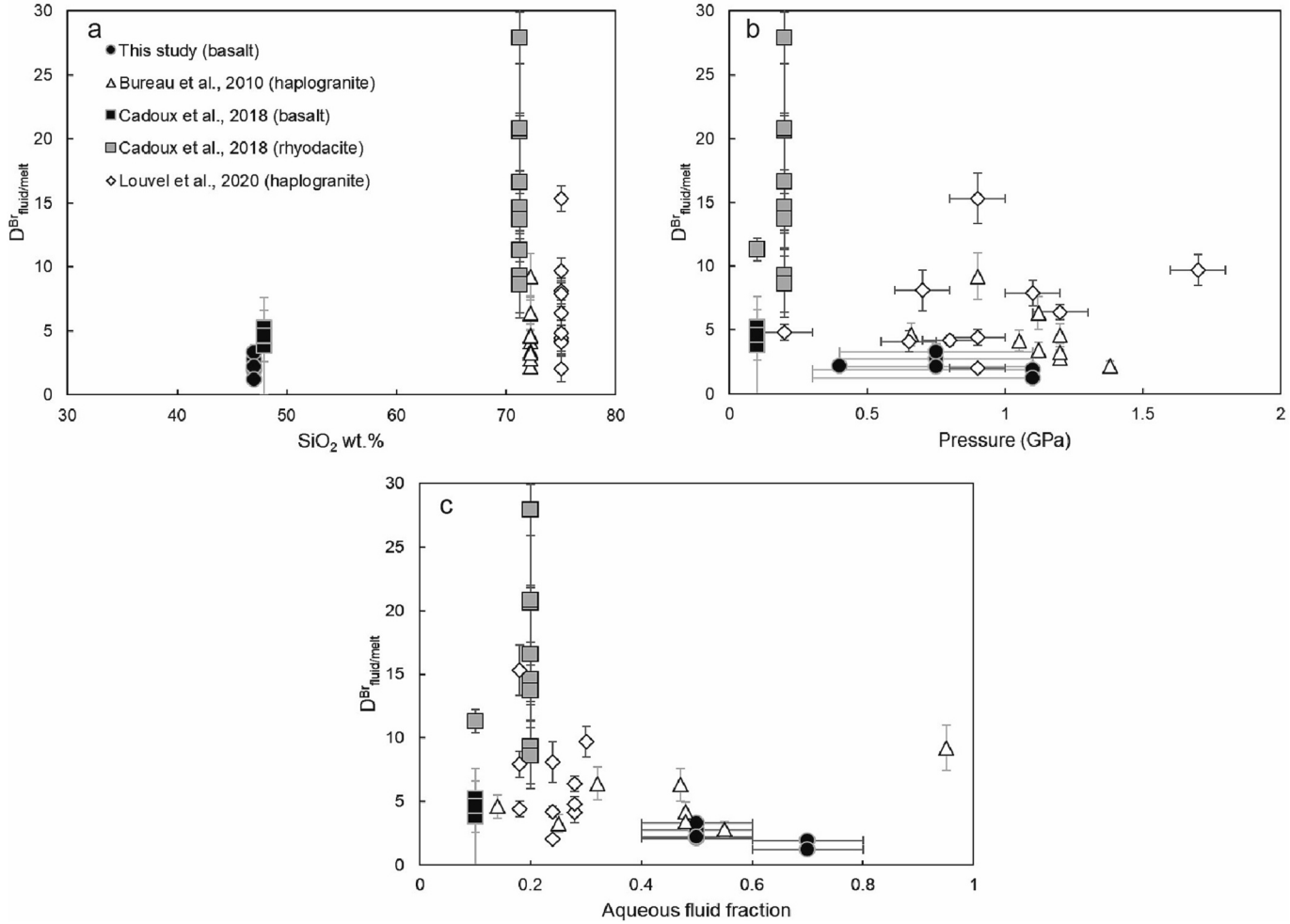

Fig. 6. Aqueous fluid-melt partition coefficients for bromine from Bureau et al. (2010) (triangle), Cadoux et al. (2018) (box), Louvel et al. (2020b) (diamond) and this study (Cpo2, Cpo3, LN22 in circles) vs. a) SiO_2 content in the silicate glass; b) vs. pressure; c) vs. aqueous fluid fraction.

haplogranite but has higher $D^{Br}_{fluid/melt}$ values. This can be best explained with the pressure trend described by Bureau et al. (2010).

As the partition coefficients for basalts are generally smaller than for SiO_2-rich melts, the data from Cadoux et al. (2018) and from this study support the pressure trend, as well as the general trend of decreasing $D^{Br}_{fluid/melt}$ with increasing water content. However, given the uncertainties and the data spreading from all discussed studies and the much stronger effect melt composition, it is not clear if pressure, melt composition, or fluid fraction have the strongest effect on the partitioning.

4.2. Bromine partitioning between basalt glass and neon

The calculated neon-melt partition coefficients in the experiments Hak1 and Mar1 are in the range of $D^{Br}_{fluid/melt} = 0.38 \pm 0.06$ and imply that Br favors to remain in the basalt liquid over partitioning into the neon, an inert fluid phase (Table 1). To the authors' knowledge there are no further studies on halogen partitioning between a silicate glass and neon or any other dry gaseous phase such as CO_2. We argue that Br has a strong affinity to bond with water but a low affinity to bond with neon which can be a good analogue for CO_2, the second major volatile degassed by volcanoes. Both neon and CO_2 do not have a strong bonding affinity to halogens. Therefore, Br tends to remain in the basaltic melt. However, partition coefficients from experiment Hak2 range from 1.16 to 1.83. This discrepancy within the neon-related experiments needs to be addressed:

We used a hydrous basalt with about 2 wt% of H_2O as starting material for the experiments of this study. In experiment Hak1 water droplets released from the hydrous basalt could be observed in the sample chamber after the last heating cycle (Fig. 1d; Fig. 5). The water droplets were visible at the end of run Hak1 and could explain the decrease of Br concentration in the neon from 3985 to 208 μg/g Br after the last heating cycle: As soon as small amounts of water appear as a third phase in the sample chamber, Br partitions from neon into water leaving the neon fluid with much lower Br concentration than in the former heating-quenching cycles.

The cell remained closed for the next experiment Hak2 but after recompression of the cell the water droplets could not be observed during the experiment Hak2. At ≥1.4 GPa and ambient temperature liquid water is not stable but instead ice VI (Wagner and Pruß, 2002). However, neither water nor ice VI were observed before and during the Hak2 experiment. In the lack of Br partitioning data between ice VI and neon we assume that not much Br can be incorporated in the structure of ice VI and that most of the Br goes back into neon when water transforms into ice during the re-compression of the sample.

The partition coefficients between basalt and (dry) neon are represented by the first two heating cycles of Hak1 (0.38 and 0.39) before water droplets were observed. The higher partition coefficients over several heating-quenching cycles in Hak2 (1.16–1.83) must be related to the presence of water. At this stage the basalt crossed the glass transition several times (heating and quenching cycles) and Br should partition from the neon back into the basalt while the system equilibrates.

Instead, Br concentrations and $D^{Br}_{neon/glass}$ remain higher than in Hak1.

A mixed fluid of "wetted" or hydrous neon probably explains the elevated concentrations and partitioning values. During heating of the Hak2 experiment neon takes up the water (initially stored in liquid droplets or ice) and increases its Br storage capacity as it becomes slightly hydrous. In Hak1 the water release from the basalt liquid has been initially prevented by the high pressure in the first cycles. After external decompression in the last cycle of Hak1 water could be released from the basalt glass. This is a very likely scenario as the water solubility in the basalt glass strongly relies on pressure (e.g., Dixon et al., 1995). As the basalt dehydrates during the melting, experiments with dry basalt would be needed to clarify Br behavior in neon.

4.3. Volcanic bromine degassing and global bromine fluxes

Bromine concentrations in natural melts, fluids, or volcanic gases are usually in the range of low μg/g. Monitoring of Br cycling, or volcanic degassing remains challenging, and so far, the data are scarce relative to e.g., the lighter halogens fluorine (F) and Cl (e.g., Webster et al., 2018). To calculate a (global) flux for volcanic halogen degassing, two methods can be applied: (1) Volatile degassing can be measured directly at active volcanoes or (2) halogen concentration in melt inclusions can be studied as a petrological approach (for detailed reviews of both methods: Wallace, 2005; Pyle and Mather, 2009; Webster et al., 2018, and references therein).

4.3.1. Volcanic halogen degassing

Halogen flux calculations from present-day emissions have been applied to accessible volcanoes – most of them are related to arc volcanism (Pyle and Mather, 2009). Due to its high concentration in volcanic gasses SO_2 is the easiest volatile to measure in volcanic plumes. Measured halogen concentrations can be scaled up using e.g., HF/SO_2 or HCl/SO_2 ratios (Wallace, 2005). For Br either HBr/HCl or HCl/SO_2 are commonly in use as ratios. However, halogen- and SO_2 degassing show large spatial variations and can vary dramatically at one volcano during different phases of activity (c.f. Edmonds et al., 2001, 2002). This can have large impacts on global flux upscaling (Pyle and Mather, 2009; Webster et al., 2018; Cadoux et al., 2022). Recent flux estimates for halogens from volcanic gas data range therefore over two orders of magnitude for F and Cl, and over four orders of magnitude for Br and iodine (Webster et al., 2018).

Several values for global Br flux from volcanic arc degassing have been calculated based on HBr measurements and the comparison to HBr/HCl or HCl/SO_2 ratios: Halmer et al. (2002) calculated $2.6–43.2 \times 10^9$ g/y, Aiuppa et al. (2005) calculated 13×10^9 g/y, Pyle and Mather (2009) calculated $5–15 \times 10^9$ g/y, and Webster et al. (2018) calculated 10.5×10^9 g/y (Table 5). Several studies on volatile degassing show that halogen degassing from non-arc volcanism is rather negligible for global flux calculations of e.g., Cl (5.5 wt% of the annual global flux) and for heavy halogens like Br (0.6 wt%; Webster et al., 2018; with data from: Gerlach, 2004; Aiuppa et al., 2009; Shinohara, 2013).

Table 5
Estimates of annual global volcanic bromine flux to the atmosphere.

HBr (Gg/year)		Study
volcanic flux		
based on SO_2 flux from the respective study	corrected with SO_2 flux from Carn et al. (2017)	
2.6–43.2	–	Halmer et al. (2002)
13	21.4	Aiuppa et al. (2005)
5–15	8–23	Pyle and Mather (2009)
10.5	14.4	Webster et al. (2018)
9	12.3	Cadoux et al. (2022)
melt inclusions		
23.5–72.9		this study

4.3.2. Global flux calculation from melt inclusions

The calculation of global halogen flux from melt inclusions compares the concentration of halogens measured in pre-eruptive melt inclusions with post-eruptive glass of the final degassed lava (e.g., Webster et al., 2018; d'Augustin et al., 2020). This approach allows to estimate volatile flux from volcanic eruption of the past. Chlorine and fluorine exsolve at low pressures with <100 MPa for Cl and < 10 MPa for F (Aiuppa et al., 2009; Webster et al., 2018). This implies late degassing of both halogens during magma ascent and a good preservation of initial Cl and F contents in pre-eruptive melt inclusions. Not much is known about the behavior of Br but the small pressure effect on melt-fluid partitioning in basalts suggests also shallow degassing of Br.

Following the method described in Wallace (2005), we can calculate an annual bromine flux q_{Br}:

$$q_{Br} = \frac{Q \times \rho_B}{c_{fl}}$$

with ρ_B as the density for basalt (2.8 g/cm^3). For the annual magma flux Q, we use a global arc magma flux of 2.5×10^{15} cm^3/y from Carmichael (2002). Instead of using Br measurements from post-erupted glasses, the bromine concentration in the fluid/degassing phase c_{fl} can be calculated as

$$c_{fl} = c_{mi} \times W \frac{D}{D+1}$$

with c_{mi} as bromine concentration in melt inclusions and D as the newly gained partition coefficient $D^{Br}_{fluid/melt}$ for aqueous fluid experiments from this study. The addition of the factor W considers that the fluid fraction in our experiments is higher than in natural systems: Experiments from this study have a fluid fraction of 25 to 45 wt%. Arc magmas can have water contents up to 20 wt%, but probably not all over the globus (Urann et al., 2022). Assuming a water content between 5 and 12 wt% would lead to a factor $W = 3$ to 7.

The amount of data for bromine concentration in melt inclusions (c_{mi}) are rather limited relative to the lighter halogens F and Cl. Webster et al. (2018) compiled a dataset of 175 measurements for Br and 4710 measurements for Cl in melt inclusions. They find that primitive arc magmas have in general Br concentrations <10 μg/g. Higher concentrations are however possible: Straub and Layne (2003) found melt inclusions with Cl concentration of 9400 μg/g from the Izu Bonin arc. According to typical Cl/Br mantle ratios of about 300, primitive melts at the Izu Bonin arc could have Br concentrations of 30 μg/g (Bureau et al., 2010). But for a global Br distribution in primitive arc magmas an average concentration of 5 μg/g is more likely (e.g., dataset from Webster et al., 2018) and is also in good agreement with other recent findings with about 3–5 μg/g Br in melt inclusions from arc basalts (Kutterolf et al., 2013; Vidal et al., 2016).

With 5 μg/g as initial average Br concentration the calculated global Br flux from arc volcanoes ranges from 23.5×10^9 g/y to 72.9×10^9 g/y in respect to the minimum and maximum values of our experimentally determined partition coefficients $D^{Br}_{fluid/glass} = 1.19$ and $D^{Br}_{fluid/glass} = 3.92$ and the water content of arc magmas. The calculated flux is higher than values from degassing data (Table 5), but these values could be underestimated as they assume a SO_2 fluxes of $14*10^{12}$ g/y (Aiuppa et al., 2005), $15*10^{12}$ g/y (Pyle and Mather, 2009), $16.8*10^{12}$ g/y (Webster et al., 2018), or $16.8*10^{12}$ g/y (Cadoux et al., 2022) for their calculations of the Br flux. Recent findings of a higher SO^2 flux of $23 \pm 2*10^{12}$ g/y (Carn et al., 2017) would lead also to higher results for corrected Br degassing values with fluxes of $21.4 *10^9$ g/y, 8–23 $*10^9$ g/y, $14.4 *10^9$ g/y, or $12.3 *10^9$ g/y, respectively (Table 5). Given all uncertainties for volatile flux estimations in general, these values for the global Br flux

and the newly calculated flux based on our experiments are in a very good agreement.

5. Conclusion

We present a new experimental dataset for Br partitioning between basalt and an aqueous fluid and between basalt and neon. To our knowledge these are the first experimental data measured in-situ for Br degassing from basalt. We calculated partition coefficients of $D^{Br}_{fluid/melt}$ = 1.19 to 3.92 at 0.4 to 1 GPa for magma degassing in water-rich magmas (aqueous fluids in equilibrated experiments). The values are in good agreement with partition coefficients from ex-situ experiments at lower pressures with basalt (Cadoux et al., 2018) and confirm a slight negative correlation with pressure, as well as a strong positive correlation with SiO_2 content.

Experiments with an inert gas analogue for CO_2 as pressure medium (neon) give partition coefficients <1 ($D^{Br}_{fluid/melt}$ = 0.38 ± 0.01 at 1.1 GPa) for magma degassing under almost dry (2 wt% water) conditions, as neon and Br have no bonding affinity. These experiments propose less Br degassing for e.g., dry intra-plate volcanism relative to hydrous eruptions in arcs, in good agreement with natural observations.

From the calculated partition coefficients for the presented anhydrous experiments and from global Br concentration values in melt inclusions from arc magmas, we calculated a global Br flux of 23.5–72.9*10^9 g/y. This flux is higher than most values calculated from active volcano degassing (Aiuppa et al., 2005; Pyle and Mather, 2009; Webster et al., 2018) but agrees well with new findings on global SO_2 degassing (Carn et al., 2017). Former calculated fluxes may be slightly underestimating the annual Br degassing.

Research support

Tobias Grützner reports financial support was provided by the European Commission.

Hélène Bureau reports financial support was provided by the French National Research Agency.

Relationships

There are no additional relationships to disclose.

Patents and intellectual property

There are no patens to disclose.

Other activities

There are no additional activities to disclose.

CRediT authorship contribution statement

Tobias Grützner: Conceptualization, Data curation, Formal analysis, Investigation, Methodology, Validation, Visualization, Writing – original draft, Writing – review & editing, Project administration, Resources. **Hélène Bureau:** Conceptualization, Funding acquisition, Investigation, Methodology, Supervision, Validation, Writing – review & editing, Project administration, Resources. **Eglantine Boulard:** Formal analysis, Investigation, Writing – review & editing. **Pascal Munsch:** Investigation, Writing – review & editing. **Nicolas Guignot:** Investigation, Methodology, Writing – review & editing. **Julien Siebert:** Investigation, Writing – review & editing. **Yoann Guarnelli:** Methodology, Resources, Writing – review & editing.

Declaration of Competing Interest

None.

Data availability

Data will be made available on request.

Acknowledgements

This project was funded by the ANR Projet de Recherche Collaborative VOLC-HAL-CLIM (Volcanic Halogens: from Deep Earth to Atmospheric Impacts), ANR-18-CE01-0018 (Hélène Bureau). Tobias Grützner is grateful for an EU Marie Skłodowska-Curie Fellowship "ExCliso" (Project ID 101017762). We thank the PSICHÉ staff at SOLEIL for their assistance. Paraskevas Parisiadis is thanked for his help with the laser heating test runs we performed at the IMPMC. We thank Marion Louvel, Richard W Thomas, and the two reviewers for their helpful comments to improve the manuscript. Editor Claudia Romano is thanked for handling the manuscript. The authors acknowledge the facilities, and the scientific and technical assistance of Microscopy Australia at the Centre of Advanced Microscopy, The Australian National University.

Appendix A. Supplementary data

Supplementary data to this article can be found online at https://doi.org/10.1016/j.chemgeo.2023.121869.

References

Aiuppa, A., Federico, C., Franco, A., Giudice, G., Gurrieri, S., Inguaggiato, S., Liuzzo, M., McGonigle, A.J.S., Valenza, M., 2005. Emission of bromine and iodine from Mount Etna volcano. Geochem. Geophys. Geosyst. 6, Q08008.

Aiuppa, A., Baker, D.R., Webster, J.D., 2009. Halogens in volcanic systems. Chem. Geol. 263, 1–8.

Balcone-Boissard, H., Baker, D.R., Villemant, B., Caudiz, J., Boudon, G., Deloule, E., 2020. Br diffusion in phonolitic melts: comparison with fluorine and chlorine diffusion. Am. Mineral. 105 (11), 1639–1646.

Bassett, W.A., 2003. High pressure-temperature aqueous systems in the hydrothermal diamond anvil cell (HDAC). Eur. J. Mineral. 15, 773–780.

Bassett, W.A., Shen, A.H., Buckum, M., 1993. A new diamond anvil cell for hydrothermal studies to 2.5 GPa and from −190°C to 1200°C. Rev. Sci. Instrum. 64, 2340–2345.

Bobrowski, N., Giuffrida, G., 2012. Bromine monoxide/Sulphur dioxide ratios in relation to volcanological observations at Mt. Etna 2006-2009. Solid Earth 3, 433–445.

Bobrowski, N., Hönninger, G., Galle, B., Platt, U., 2003. Detection of bromin monoxide in a volcanic plume. Nature 423, 273–276.

Borchert, M., Wilke, M., Schmidt, C., Rickers, K., 2009. Partitioning and equilibration of RB and Sr between silicate melts and aqueous fluids. Chem. Geol. 259, 39.

Boyd, F.R., England, J.L., 1960. Apparatus for phase-equilibrium measurements at pressures up to 50 kilobars and temperatures up to 1750 °C. J. Geophys. Res. 65, 741–748.

Bureau, H., Keppler, H., 1999. Complete miscibility between silicate melts and hydrous fluids in the upper mantle: experimental evidence and geochemical implications. Earth Planet. Sci. Lett. 165 (2), 187–196.

Bureau, H., Keppler, H., Métrich, N., 2000. Volcanic degassing of bromine and iodine: experimental fluid/melt partitioning data and applications to stratospheric chemistry. Eart Planet. Sci. Lett. 5612, 1–10.

Bureau, H., Métrich, N., 2003. An experimental study of bromine behaviour in water-saturated silicic melts. Geochim. Cosmochim. Acta 67, 1689–1697.

Bureau, H., Foy, E., Raepsaet, C., Somogyi, A., Munsch, P., Simon, G., Kubsky, S., 2010. Bromine cycle in subduction zones through in situ Br monitoring in diamond anvil cells. Geochim. Cosmochim. Acta 74, 3839–3850.

Bureau, H., Auzende, A.-L., Marocchi, M., Raepsaet, C., Munsch, P., Testemale, D., Mézouar, M., Kubsky, S., Carrière, M., Ricolleau, A., Fiquet, G., 2016. Modern and past volcanic degassing of Iodine. Geochim. Cosmochim. Acta 173, 114–125.

Cadoux, A., Iacono-Marziano, G., Scaillet, B., Aiuppa, A., Mather, T.A., Pyle, D.M., Deloule, E., Gennaro, E., Paonita, A., 2018. The role of melt composition on aqueous fluid vs. silicate melt partitioning of bromine in magmas. Earth Planet. Sci. Lett. 498, 450–463.

Cadoux, A., Tegtmeier, S., Aiuppa, A., 2022. Natural halogen emission to the atmosphere: sources, flux, and environmental impact. Elements 18 (1), 27–33.

Carmichael, I.S.E., 2002. The andesite aqueduct: perspectives on the evolution of intermediate magmatism in west-central (105-998W) Mexico. Contrib. Mineral. Petrol. 143, 641–663.

Carn, S.A., Fioletov, V.E., McLinden, C.A., Li, C., Krotkov, N.A., 2017. A decade of global volcanic SO_2 emissions measured from space. Sci. Rep. 7 (1), 1–12.

Chervin, J.C., Canny, B., Besson, J.M., Pruzan, P., 1995. A diamond anvil cell for IR microspectroscopy. Rev. Sci. Instrum. 66 (3), 2595–2598.

Chervin, J.C., Canny, B., Mancinelli, M., 2001. Ruby-spheres as pressure gauge for optically transparent high pressure cells. High Pressure Res. 21, 305–314.

Cochain, B., Sanloup, C., de Grouchy, C., Crépisson, C., Bureau, H., Leroy, C., Kantor, I., Irifune, T., 2015. Bromine speciation in hydrous silicate melts at high pressure. Chem. Geol. 404, 18–26.
Couzinet, B., Dahan, N., Hamel, G., Chervin, J.C., 2003. Optically monitored high-pressure gas loading apparatus for diamond anvil cells. High Pressure Res. 23, 409–415.
d'Augustin, T., Balcone-Boissard, H., Boudon, G., Martel, C., Deloule, E., Bürckel, P., 2020. Evidence for an active, transcrustal magma system in the last 60 ka and eruptive degassing budget (H_2O, CO_2, S, F, Cl, Br): the case of dominica. Geochem. Geophys. Geosyst. 21 e2020GC009050.
Daniel, J.S., Solomon, S., Portmann, R.W., 1999. Stratospheric ozone destruction: The importance of bromine relative to chlorine. J. Geophys. Res. 104, 23871–23880.
Dixon, J.E., Stolper, E.M., Holloway, J.R., 1995. An experimental study of water and carbon dioxide solubilities in Mid-Ocean ridge basaltic liquids. Part I: calibration and solubility models. J. Petrol. 36, 1607–1631.
Dorogokpets, P.I., Dewaele, A., 2007. Equations of state of MgO, Au, Pt, NaCl-B1, and NaCl-B2: internally consistent high-temperature pressure scales. High Pressure Res. 27, 431–446.
Edmonds, M., Pyle, D., Oppenheimer, C., 2001. A model of degassing at the Soufrière Hills Volcano, Montserrat, West Indies, based on geochemical data. Earth Planet. Sci. Lett. 186, 159–173.
Edmonds, M., Pyle, D.M., Oppenheimer, C., 2002. HCl emissions at Soufrière Hills Volcano, Montserrat, West Indies, during a second phase of dome building: November 1999 to October 2000. Bull. Volcanol. 64, 21–30.
Fehn, U., 2012. Tracing crustal fluids: applications of natural ^{129}I and ^{36}C. Annu. Rev. Earth Planet. Sci. 40, 45–67.
Gerlach, T.M., 2004. Volcanic source of tropospheric ozone-depleting trace gases. Geochem. Geophys. Geosyst. 5, Q09007. https://doi.org/10.1029/2004GC000747.
Gutmann, A., Bobrowski, N., Roberts, T.J., Rüdiger, J., Hoffmann, T., 2018. Advances in bromine speciation in volcanic plumes. Front. Earth Sci. 6, 213.
Halmer, M.M., Schmincke, H.U., Graf, H.F., 2002. The annual volcanic gas input into the atmosphere, in particular into the stratosphere: a global dataset for the past 100 years. J. Volcanol. Geotherm. Res. 115, 511–528.
Kutterolf, S., Hansteen, T.H., Appel, K., Freundt, A., Krüger, K., Pérez, W., Wehrmann, H., 2013. Combined bromine and chlorine release from large explosive volcanic eruptions: a threat to stratospheric ozone? Geology 41 (6), 707–710.
Leroy, C., Bureau, H., Sanloup, C., Raepsaet, C., Glazirin, K., Munsch, P., Harmand, M., Prouteau, G., Khodja, H., 2019. Xenon and iodine behaviour in magmas. Earth Planet. Sci. Lett. 522, 144–154.
Louvel, M., Cadoux, A., Brooker, R.A., Proux, O., Hazemann, J.-L., 2020a. New insights on Br speciation in volcanic glasses and structural controls on halogen degassing. Am. Mineral. 105, 795–802.
Louvel, M., Sanchez-Valle, C., Malfait, W.J., Pokrovski, G.S., Borca, C.N., Grolimund, D., 2020b. Bromine speciation and partitioning in slab-derived aqueous fluids and silicate melts and implications for halogen transfer in subduction zones. Solid Earth 11, 1145–1161.
Mosbah, M., Clocchiatti, R., Michaud, V., Piccot, D., Chevallier, P., Legrand, F., Als Nilsen, G., Grübel, G., 1995. Micro PIXE and micro SXRF: comparison of the two methods and application to glass inclusions from Vulcano (Eolian Islands – Italy). Nucl. Inst. Methods Phys. Res. B 104, 481–488.
Munsch, P., Bureau, H., El Yakoubi, M., Khodja, H., Zaitsev, A., 2015. The use of ^{13}C diamond as pressure and temperature sensor for diamond-anvil-cell experiments. Eur. J. Mineral. 27, 365–375.
Newsom, H.E., 1995. Composition of the solar system, planets meteorites and major terrestrial reservoirs. In: Ahrens, T.J. (Ed.), Global Earth Physics. American Geophysical Union, Washington, DC, pp. 159–189.
Pichavant, M., Mysen, B.O., Macdonald, R., 2002. Source and H_2O content of high-MgO magmas in island arc settings: an experimental study of a primitive calc-alkaline basalt from St. Vincent, Lesser Antilles arc. Geochim. Cosmochim. Acta 66, 2193–2209.
Prescher, C., Prakapenka, V.B., 2015. DIOPTAS: a program for reduction of two-dimensional X-ray diffraction data and data exploration. High Pressure Res. 35 (3), 223–230.
Pyle, D.M., Mather, T.A., 2009. Halogens in igneous processes and their fluxes to the atmosphere and oceans from volcanic activity: a review. Chem. Geol. 263, 110–121.
Roberts, T.J., Vignelles, D., Liuzzo, M., Giudice, G., Aiuppa, A., Coltelli, M., Salerno, G., Chartier, M., Couté, B., Berthet, G., Lurton, T., Dulac, F., Renard, J.-B., 2018. The primary volcanic aerosol emission from Mt Etna: Size-resolved particles with SO_2 and role in plume reactive halogen chemistry. Geochim. Cosmochim. Acta 222, 74–93.
Rocholl, A.B.E., Simon, K., Jochum, K.P., Gehann, R., Kramar, U., Luecke, W., Molzahn, M., Pernicka, E., Seufert, M., Spettel, B., Stummeier, J., 1997. Chemical characterization of NIST silicate glass certified reference material SRM 610 by ICPMS, TIMS, LIMS, SSMS, INAA, AAS and PIXE. Geostand. Newslett. 21-1, 101–114.
Rousseau, R.M., 2021. Detection Limit and estimate of uncertainty of analytical XRF results. Rigaku J. 18 (2), 33–47.
Shen, G., Wang, Y., Dewaele, A., Wu, C., Fratanduono, D.E., Eggert, J., Klotz, S., Dziubek, K.F., Loubeyre, P., Fat'yanov, O.V., Asimov, P.D., Mashimo, T., Wentzcovitch, R.M.M., 2020. Toward an international practical pressure scale: a proposal for an IPPS ruby gauge (IPPS-Ruby2020). High Pressure Res. 40 (3), 299–314.
Shinohara, H., 2013. Volatile flux from subduction zone volcanoes: insights from a detailed evaluation of the fluxes from volcanoes in Japan. J. Volcanol. Geotherm. Res. 268, 46–63.
Sinnhuber, B.-M., Sheode, N., Sinnhuber, M., Chipperfield, M.P., Feng, W., 2009. The contribution of anthropogenic bromine emissions to past stratospheric ozone trends: a modelling study. Atmos. Chem. Phys. 9 (8), 2863–2871.
Solé, A., Papillon, E., Cotte, M., Walter, Ph., Susini, J., 2007. A multiplatform code for the analysis of energy-dispersive X-ray fluorescence spectra. Spectrochim. Acta, Part B 62, 63–68.
Straub, S.M., Layne, G.D., 2003. The systematics of chlorine, fluorine and water in Izu arc front volcanic rocks: implications for volatile recycling in subduction zones. Geochim. Cosmochim. Acta 67, 4179–4203.
Toby, B.H., Von Dreele, R.B., 2013. GSAS-II: the genesis of a modern open-source all purpose crystallography software package. J. Appl. Crystallogr. 46 (2), 544–549.
Urann, B.M., Le Roux, V., Jagoutz, O., Müntener, O., Behn, M.D., Chin, E.J., 2022. High water content of arc magmas recorded in cumulates from subduction zone lower crust. Nat. Geosci. 15, 501–508.
Vidal, C.M., Métrich, N., Komorowski, J.-C., Pratomo, I., Michel, A., Kartadinata, N., Robert, V., Lavigne, F., 2016. The 1257 Samalas eruption (Lombok, Indonesia): the single greatest stratospheric gas release of the Common Era. Sci. Rep. 6, 34868.
Wagner, W., Pruß, A., 2002. The IAPWS formulation 1995 for the thermodynamic properties of ordinary water substance for general and scientific use. J. Phys. Chem. Ref. Data Monogr. 31, 387.
Wallace, P.J., 2005. Volatiles in subduction zone magmas: concentrations and fluxes based on melt inclusion and volcanic gas data. J. Volcanol. Geotherm. Res. 140, 217–240.
Webster, J.D., de Vivo, B., 2002. Experimental and modeled solubilities of chlorine in aluminosilicate melts, consequences of magma evolution, and implications for exsolution of hydrous chloride melt at Mt. Somma–Vesuvius. Am. Mineral. 87, 1046–1061.
Webster, J.D., Kinzler, R.J., Mathez, E.A., 1999. Chloride and water solubility in basalt and andesite melts and implications for magmatic degassing. Geochim. Cosmochim. Acta 63, 729–738.
Webster, J.D., Baker, D.R., Aiuppa, A., 2018. Halogens in Mafic and intermediate-silica content magmas. In: Harlov, D., Aranovich, L. (Eds.), The Role of Halogens in Terrestrial and Extraterrestrial Geochemical Processes. Springer Geochemistry. Springer, Cham.
Witt, M.L.I., Mather, T.A., Pyle, D.M., Aiuppa, A., Bagnato, E., Tsanev, V.I., 2008. Mercury and halogen emissions from Masaya and Telica volcanoes, Nicaragua. J. Geophys. Res. 113, B06203.